A Prokaryotic Membrane Sculpting BAR Domain Protein

Daniel A. Phillips[1*], Lori A. Zacharoff[2*], Cheri M. Hampton[3], Grace W. Chong[4], Anthony P. Malanoski[5], Lauren Ann Metskas[6], Shuai Xu[2], Lina J. Bird[5], Brian J. Eddie[5], Grant J. Jensen[6,7], Lawrence F. Drummy[3], Mohamed Y. El-Naggar[2,4,8], and Sarah M. Glaven[5]

[1]American Society for Engineering Education, Washington, DC, USA.
[2]University of Southern California, Department of Physics and Astronomy, Los Angeles, CA 90089
[3]Materials and Manufacturing Directorate, Air Force Research Laboratory, Wright-Patterson Air Force Base, WPAFB, OH, USA.
[4]University of Southern California, Department of Biological Sciences, Los Angeles, CA 90089
[5]Center for Bio/Molecular Science and Engineering, Naval Research Laboratory, Washington, DC, USA.
[6]California Institute of Technology, Division of Biology and Biological Engineering, Pasadena, CA 91125
[7]California Institute of Technology, Howard Hughes Medical Institute, Pasadena, CA 91125
[8]University of Southern California, Department of Chemistry, Los Angeles, CA 90089

[*]These authors contributed equally to this work

Send all correspondence to:
Daniel A. Phillips
Daniel.phillips.ctr@nrl.navy.mil
4555 Overlook Ave.
Washington, DC 20375

Lori Zacharoff
zacharof@usc.edu
920 Bloom Walk
SSC, 215C
Los Angeles, CA 90089

Summary Paragraph

Bin/Amphiphysin/RVS (BAR) domain proteins belong to a ubiquitous superfamily of coiled-coil proteins that influence membrane curvature in eukaryotes and are associated with vesicle biogenesis, vesicle-mediated protein trafficking, and intracellular signaling[1-6]. BAR domain proteins have not been identified in bacteria, despite certain organisms displaying an array of membrane curvature phenotypes[7-16]. Here we identify a prokaryotic BAR domain protein, BdpA, from *Shewanella oneidensis* MR-1, an iron reducing bacterium known to produce redox active membrane vesicles and micrometer-scale membrane extensions. BdpA is required for uniform size distribution of outer membrane vesicles and is responsible for scaffolding outer membrane extensions (OMEs) into membrane structures with consistent diameter and curvature. While a strain lacking BdpA produces OMEs, cryogenic transmission electron microscopy reveals more lobed, disordered OMEs rather than the membrane tubes produced by the wild type strain. Overexpression of BdpA promotes OME formation even during planktonic conditions where *S. oneidensis* OMEs are less common. Heterologous expression also results in OME production in *Marinobacter atlanticus* CP1 and *Escherichia coli*. Based on the ability of BdpA to alter membrane curvature *in vivo*, we propose that BdpA and its homologs comprise a newly identified class of prokaryotic BAR (P-BAR) domains that will aid in identification of putative P-BAR proteins in other bacterial species.

Introduction

Eukaryotic Bin/Amphiphysin/Rvs (BAR) domain-containing proteins generate membrane curvature through electrostatic interactions between positively charged amino acids and negatively charged lipids, scaffolding the membrane along the intrinsically

24 curved surface of the antiparallel coiled-coil protein dimers[17-20]. Some BAR domain-
25 containing proteins, such as the N-BAR protein BIN1, contain amphipathic helical wedges
26 that insert into the outer membrane leaflet and can assist in membrane binding[21]. Other
27 BAR domains can be accompanied by a membrane targeting domain, such as PX for
28 phosphoinositide binding[22,23], in order to direct membrane curvature formation at specific
29 sites, as is the case with sorting nexin BAR proteins[4]. The extent of accumulation of BAR
30 domain proteins at a specific site can influence the degree of the resultant membrane
31 curvature[24], and tubulation events arise as a consequence of BAR domain
32 multimerization in conjunction with lipid binding[25]. Interactions between BAR domain
33 proteins and membranes resolve membrane tension, promote membrane stability, and
34 aid in localizing cellular processes, such as actin binding, signaling through small
35 GTPases, membrane vesicle scission, and vesicular transport of proteins[1,26,27]. Despite
36 our knowledge of numerous eukaryotic BAR proteins spanning a variety of modes of
37 curvature formation, membrane localizations, and subtypes (N-BAR, F-BAR, and I-BAR),
38 characterization of a functional prokaryotic BAR domain protein has yet to be reported.

39 Bacterial cell membrane curvature can be observed during the formation of outer
40 membrane vesicles (OMV) and outer membrane extensions (OME). OMV formation is
41 ubiquitous and has many documented functions[9]. OMEs are less commonly observed,
42 remain attached to the cell, and various morphologies can be seen extending from single
43 cells including *Myxococcus xanthus*[14,15], flavobacterium strain Hel3_A1_48[8], *Vibrio*
44 *vulnificus*[10], *Francisella novicida*[28], *Shewanella oneidensis*[7,29-31], and as cell-cell
45 connections in *Bacillus subtilis*[32-34] and *Eschericia coli*[35]. Several bacterial proteins have
46 demonstrated membrane tubule formation capabilities *in vitro*[16,36-40], but despite the

47 growing number of reports, proteins involved in shaping bacterial membranes into
48 OMV/Es have yet to be identified. Recently, researchers have begun to suspect that OMV
49 and OME formation has some pathway overlap[8], and it is proposed that proteins are
50 necessary to stabilize these structures[13].

51 *Shewanella oneidensis* is a model organism for extracellular electron transfer
52 (EET), a mode of respiration whereby electrons traverse the inner membrane, periplasm,
53 and outer membrane via multiheme cytochromes to reach exogenous insoluble terminal
54 electron acceptors, such as metals and electrodes[41,42]. It is also known to produce redox-
55 active OMVs[43] and OMEs coated with mulitheme cytochromes, particularly upon surface
56 attachment[7,30,43]. However, little is known about their formation mechanism, control of
57 shape or curvature, and electrochemical properties that influence EET function.

58 **Results and Discussion**

59 ***S. oneidensis* OMVs are redox-active and enriched with BdpA**

60 OMVs were purified from cells grown in batch cultures to characterize the redox
61 features and unique proteome of *S. oneidensis* OMVs, as well as to identify putative
62 membrane shaping proteins. Cryogenic transmission electron microscopy (cryo-TEM)
63 tomography reconstruction slices of the purified samples showed uniform OMVs with the
64 characteristic single membrane phenotype and an approximate diameter of 200 nm (Fig.
65 1a). Previous measurements suggest OMVs can reduce extracellular electron
66 acceptors[43] and that vesicles from *G. sulfurreducens* can mediate electron transfer[44].
67 Electrochemical activity of multiheme cytochrome complex MtrCAB and their ability to
68 mediate micrometer-scale electron transport has been characterized in whole cells[45], but
69 no electrochemical characterization of OME/Vs has been reported that link activity to

70 multiheme cytochromes. Here, electrochemical measurements of isolated OMVs were
71 performed to determine if purified OMVs maintain the redox features when detached from
72 cells. Cyclic voltammetry (CV) of isolated membrane vesicles adhered to a gold electrode
73 via self-assembled monolayers show redox activity demonstrating electron transfer to and
74 from the electrode interface (Fig. 1b). The first derivative (Fig. 1b inset) revealed a
75 prominent peak with a midpoint potential of 66 mV and a smaller peak at -25 mV versus
76 a standard hydrogen reference electrode (SHE). This midpoint potential is consistent with
77 the characteristics of multiheme cytochromes such as MtrC/OmcA from previous
78 microbial electrochemical studies[45,46], suggesting that the extracellular redox molecules
79 of the cellular outer membrane extends to OMVs.

80 The proteome of the OMVs was compared to the proteome of purified outer
81 membranes extracted from whole cells. Using a label-free quantification method[47],
82 significant differences in the ratio of individual proteins in the vesicle to the outer
83 membrane could be computed (log fold change) (Fig 1c). The proteome of the purified
84 OMVs showed ~300 proteins were significantly enriched in the vesicles as compared to
85 the outer membrane, and ~300 proteins were significantly excluded from the vesicles
86 (Fig. 1c). MtrCAB cytochromes were neither significantly enriched nor excluded from the
87 vesicles, consistent with the interpretation that vesicles could extend the respiratory
88 surface area. Active protein sorting into eukaryotic vesicles is a coordinated process
89 involving a protein sorting signal, localized membrane protein recruitment, initiation of
90 membrane curvature induction, and coating nascent vesicles with membrane scaffolds[48].
91 Several proteins significantly enriched in the vesicles might contribute to OMV formation,
92 such as murein transglycosylase, the peptidoglycan degradation enzyme holin, cell

93 division coordinator CpoB, and a highly enriched putative BAR domain-containing protein
94 encoded by the gene at open reading frame SO_1507, hereafter named BAR domain-
95 like protein A (BdpA) (Fig. 1d).

96 Vesicle enrichment of BdpA led us to the hypothesis that BdpA could be involved
97 in membrane shaping of OMVs based on the role of such proteins in eukaryotes. The C-
98 terminal BAR domain of BdpA is predicted to span an alpha-helical region from AA 276-
99 451 (E-value = 2.96e-03); however, since the identification of the protein is based on
100 homology to the eukaryotic BAR domain consensus sequence (cd07307), it is possible
101 that the BAR domain region extends beyond these bounds (Fig. 1d). Coiled coil
102 prediction[49] suggests BdpA exists in an oligomeric state of antiparallel alpha-helical
103 dimers, as is the case for all known BAR domain proteins[18,50-52]. BdpA has an N-terminal
104 signal peptide with predicted cleavage sites between amino acids 22-23, suggesting non-
105 cytoplasmic localization (Fig. 1d). A galactose-binding domain-like region positioned
106 immediately downstream of the signal peptide supports lipid targeting activity seen in
107 other BAR domain proteins, such as the eukaryotic sorting nexins[3] which have phox (PX)
108 domains that bind phosphoinositides[53]. The *S. oneidensis* rough-type lipopolysaccharide
109 (LPS) contains 2-acetamido-2-deoxy-D-galactose[54], which suggests possible localization
110 of the protein to the outer leaflet of the outer membrane.

111 **BdpA controls size distribution of vesicles**

112 To determine whether BdpA influences vesicle morphology, OMVs were harvested
113 from wild type (WT) cells and cells in which the gene for BdpA had been deleted (Δ*bdpA*),
114 and their diameters were measured by dynamic light scattering (DLS). WT OMVs (n=11)
115 had a median diameter of 190 nm with little variability in the population (±21 nm), while

116 the diameters of Δ*bdpA* OMVs (n=9) were distributed over a wider range with a median
117 value of 280 nm ± 131 nm (Fig 2a). The data suggest BdpA controls vesicle diameter in
118 membrane structures *ex vivo*, potentially acting by stabilizing OMVs. OMV frequency and
119 size distribution was also measured in live cultures using a perfusion flow imaging
120 platform and the membrane stain FM 4-64, as described previously[29]. *S. oneidensis*
121 strains were monitored for OME/V production over the course of 5 hours (>5 fields of view
122 per replicate, n=3). Spherical membrane stained extracellular structures were classified
123 as OMVs, while larger aspect ratio (i.e. length greater than the width) structures were
124 classified as OMEs. The duration of time-lapse imaging allowed tracking the progression
125 of an OME/V over time. It was possible to quantify the proportion of cells producing 'large'
126 vesicles, defined as those where the membrane was clearly delineated from the interior
127 of the vesicles, typically >300 nm. Δ*bdpA* cells produced significantly more large vesicles
128 compared to WT cells (Fig. 2b) even though both the overall frequency of vesiculation
129 and extensions were the same (Fig. 2c). The size of *S. oneidensis* vesicles was more
130 discrete than vesicles produced by other bacteria[55,56] that do not contain a BdpA homolog,
131 making it likely that BdpA is responsible for precise regulation of vesicle size. Previous
132 studies showed that OMEs transition between large vesicles and OMEs over time[29].
133 BdpA appears to be involved in this transition due to the increased frequency of large
134 vesicles from Δ*bdpA* cells.

135 **BdpA constrains membrane extension morphology**

136 The median diameter of the OMVs is also the apparent maximum diameter
137 observed in outer membrane extensions[29] suggesting BdpA influences membrane
138 morphologies of both structures. As with the vesicles, WT and Δ*bdpA* cells made the

139 same number of extensions in perfusion flow conditions (Fig. 2c). The resolution of
140 fluorescence microscopy was insufficient to identify morphological differences between
141 OMEs. To minimize sample processing of unfixed OMEs for cryo-TEM sample
142 preparation, cells were deposited onto a glass coverslip instead of a perfusion flow
143 chamber. BdpA was also expressed from a 2,4-diacetylphloroglucinol (DAPG)-inducible
144 promoter[57] (P_{PhlF}-BdpA) in the Δ*bdpA* strain containing the plasmid p452-*bdpA*. After 3
145 hours post deposition on cover glass, OMEs can be seen extending from WT, Δ*bdpA*,
146 and Δ*bdpA* p452-*bdpA* cells (Fig. 3, Supplemental Fig. 1, 5 fields of view, n=3). Similar to
147 perfusion flow experiments (Fig. 2c), no statistically significant difference in the overall
148 frequency of OME production was observed between the cells in static cultures.

149 Cryo-TEM was used to assess any morphological differences between the OMEs
150 in each of the strains at the ultrastructural level. *S. oneidensis* OMEs from unfixed WT,
151 Δ*bdpA,* and Δ*bdpA* p452-*bdpA* strains were visualized at 90 minutes (Supplemental Fig.
152 2) and 3 hours (Fig. 3) post deposition onto EM grids. At 90 minutes, WT OME
153 phenotypes appeared narrow, tubule-like, and seldom interspersed with lobed regions
154 (Supplemental figure 2a). In Δ*bdpA* OMEs, lobed regions are prevalent with irregular
155 curvature (Supplemental figure 2b). Several narrow Δ*bdpA* p452-*bdpA* OMEs evenly
156 interspersed with slight constriction points or "junction densities" were observed extending
157 from a single cell (Supplemental Fig. 2c), suggesting that BdpA expression rescues the
158 phenotype by constricting and ordering OMEs into narrow tubules. By 3 hours post
159 inoculation, images of WT cells consistently show narrow, tubule-like OMEs (Fig. 3b,
160 n=31). The Δ*bdpA* OMEs generally appear as lobed, disordered vesicle chains with
161 irregular curvature, and vesicles can be observed branching laterally from lobes on the

162 extensions (Fig. 3b, n=13). Nascent WT OMEs from previous studies also exhibited
163 lateral branching of vesicles and lobes, but they exhibited uniform curvature and diameter
164 between lobes and were observed immediately following OME formation[29]. Tubules were
165 not observed in any Δ*bdpA* OMEs at 3 hours. OMEs from Δ*bdpA* p452-*bdpA* cells appear
166 as a narrow tubules of a uniform curvature or as ordered vesicle chains (Fig. 3b, n=3).

167 **Expression of BdpA results in OMEs during planktonic growth**

168 *S. oneidensis* OMEs are more commonly observed during surface attachment
169 rather than planktonic cultures[7,29]. BAR domain proteins can directly promote tubule
170 formation from liposomes *in vitro*[24], so inducing expression of an additional copy of the
171 *bdpA* gene prior to attachment could result in OME formation even during planktonic
172 growth. Growth curves were similar in cultures with the pBBR1-mcs2 empty vector in
173 either of the WT (MR-1 pBBR1-mcs2) or Δ*bdpA* (Δ*bdpA* pBBR1-mcs2) background
174 strains, but induction of *bdpA* in Δ*bdpA* p452-*bdpA* cells at higher concentrations of 1.25
175 and 12.5 μM 2,4-diacetylphloroglucinol affected the growth rate (Supplemental figure 3).
176 Planktonic cultures inoculated from overnight cultures were induced with 12.5 μM DAPG
177 for 1 hour, labeled with FM 4-64, and imaged by confocal microscopy. Neither WT (Fig.
178 4) nor MR-1 pBBR1-mcs2 exposed to 12.5 μM DAPG (not shown) produced OMEs
179 immediately following deposition onto cover glass. However, 12.5 μM DAPG-induced *S.*
180 *oneidensis* MR-1 p452-*bdpA* cells displayed OMEs immediately, ranging between 1-7
181 extensions per cell (Figure 4, Supplemental video 1). OME formation combined with
182 growth rate data suggests *bdpA* expression in planktonic cultures redirects membrane
183 production necessary for cell division into OMEs. The ultrastructure of OMEs resulting
184 from expression of *bpdA* from MR-1 p452-*bdpA* cells was examined by cryo-TEM, but in

185 this case samples from planktonic cultures were vitrified on EM grids after induction rather
186 than incubation during induction on the EM grids. OMEs appear as tubule-like segments
187 interspersed with pearled regions proximal to the main cell body (Fig. 4b). OMEs from
188 the MR-1 p452-*bdpA* strain are observed as thin, tubule-like outer membrane vesicle
189 chains, suggesting BdpA involvement in the constriction of the larger outer membrane
190 vesicle chains into longer, tubule-like extensions with more evenly interspersed junction
191 densities. The BdpA OME phenotype more closely resembles membrane tubules formed
192 by the F-BAR protein Pacsin1 from eukaryotic cells, showing a mixture of tubule regions
193 interspersed with pearled segments[58,59].

194 **BdpA-mediated membrane extensions in *Marinobacter atlanticus* CP1 and *E. coli*.**

195 To test the effect of expressing BdpA in an organism with no predicted BAR
196 domain-containing proteins and no apparent OME production, BdpA was expressed in
197 *Marinobacter atlanticus* CP1[60]. *Marinobacter* and *Shewanella* are of the same
198 phylogenetic order (Alteromonadales) and have been used for heterologous expression
199 of other *S. oneidensis* proteins, such as MtrCAB[61,62]. Upon exposure to DAPG, *M.*
200 *atlanticus* containing the p452-*bdpA* construct (CP1 p452-*bdpA*) form membrane
201 extensions (Figure 4). OMEs ranged from small membrane blebs to OME tubules
202 extending up to greater than 10 μm in length from the surface of the cell (Supplemental
203 Fig. 4). As noted previously, variation in the tubule phenotypes are commonly seen in
204 tubules from eukaryotic F-BAR proteins[58,59], showing possible mechanistic overlap of
205 mutable membrane curvature functionalities between these two separate BAR domain
206 proteins.

207 In previous membrane curvature formation experiments with eukaryotic BAR
208 domain proteins, localized BAR domain protein concentrations affected the resultant
209 shape of the membranes, ranging from bulges to tubules and branched, reticular tubule
210 networks at the highest protein densities[63-65]. We predicted that expression of BdpA in
211 cells optimized for protein overexpression, such *E. coli* BL21(DE3), would show OMEs
212 resembling structures previously observed from eukaryotic BAR protein experiments *in*
213 *vitro*. While the uninduced *E. coli* BL21(DE3) p452-*bdpA* cells had uniform, continuous
214 cell membranes similar to those of plasmid-free BL21(DE3) cells under the conditions
215 tested, *E. coli* BL21(DE3) cells containing the p452-*bdpA* vector induced with DAPG had
216 outer membrane extensions and vesicles (Figure 4). When visualized over time, OMEs
217 progressed towards a network of reticular membrane structures extending from the cell
218 (Fig. 4c). After 30 minutes, additional membrane blebs were observed that developed
219 into elongated OMEs by 60 minutes. Growth of *E. coli* OMEs was coincident with
220 shrinking of the cell body (from initial cell length = 4.457 μm to 3.479 μm at 60 minutes),
221 supporting direct membrane sculpting activity of BdpA.

222 **P-BAR: a new BAR domain subtype**

223 The discovery of a novel, functional BAR domain protein in prokaryotes provokes
224 questions into the evolutionary origin of BAR domains, such as whether the BdpA BAR
225 domain in *Shewanella* arose as a result of convergent evolution, a horizontal gene
226 transfer event, or has a last common ancestor across all domains of life. BdpA homologs
227 were identified by PSI-BLAST in several other organisms, ranging from other species of
228 *Shewanella* to *Alishewanella*, *Rheinheimera*, and *Cellvibrio* (Supplemental Fig. 5). The
229 current BAR domain pfam Hidden Markov Model (HMM) prediction analysis identified

230 BAR domain features in only 5 of the 52 prokaryotic homologs despite greater than 90%
231 homology to *S. oneidensis* BdpA. Functional analysis will be necessary to determine if
232 these homologs contain unpredicted BAR domains and merit inclusion in the generation
233 of a new BAR domain pfam seed alignment. The resultant alignment was used to
234 generate a maximum likelihood phylogenetic tree showing evolutionary relatedness of
235 BdpA orthologs to the BAR domain prediction sequences (Supplemental Fig. 5). The 5
236 BdpA orthologs predicted to contain a BAR domain based on the current model were
237 subsequently aligned with representative known BAR proteins from the various BAR
238 domain subtypes (N-BAR, F-BAR, and I-BAR)[66]. BdpA and its prokaryotic orthologs
239 cluster separately from the eukaryotic BAR proteins in their own distinct clade (Fig. 5),
240 suggesting that while BdpA contains a functional BAR domain, it represents its own class
241 of BAR domain, hereafter named P-BAR (Prokaryotic BAR). It seems likely that the P-
242 BAR domain arose as a result of horizontal gene transfer from a eukaryote due to the
243 prevalence of eukaryotic coiled-coil proteins with predicted homology to BdpA after 2
244 iterations of PSI-BLAST. However, the branch lengths and low bootstrap values
245 supporting the placement of P-BAR relative to other BAR domain subtypes make it
246 challenging to directly infer the evolutionary history of P-BAR domains. Discovery of other
247 putative P-BAR proteins would help to build this analysis, and if future comparative
248 proteomics analysis of OME/Vs demonstrates overlapping activity of BdpA with
249 preferential cargo loading into OME/Vs, it could hint at the evolutionary origins of vesicle-
250 based protein trafficking. Conservation of BAR domain proteins supports the notion that
251 three-dimensional organization of proteins in lipid structures is as important to

252 prokaryotes as it is eukaryotes, and suggests additional novel P-BAR proteins are waiting
253 to be discovered.

254

255 **Methods**

256 **Bacterial strains, plasmids, and medium** The bacterial strains used in this study can
257 be found in Supplemental Table 1. *S. oneidensis* strains were grown aerobically in Luria
258 Bertani (LB) media at 30˚C with 50 µg/mL kanamycin when maintaining the plasmid. To
259 observe membrane extensions, cells were centrifuged and resuspended in a defined
260 media comprised of 30 mM Pipes, 60 mM sodium DL-lactate as an electron donor, 28mM
261 NH4Cl, 1.34 mM KCl, 4.35 mM NaH2PO4, 7.5 mM NaOH, 30 mM NaCl, 1mM MgCl2, 1
262 mM CaCl2, and 0.05 mM ferric nitrilotriacetic acid[30]. *Marinobacter atlanticus* CP1 strains
263 were grown in BB media (50% LB media, 50% Marine broth) at 30˚C with 100 µg/mL
264 kanamycin to maintain the plasmids as described previously[60].

265 Inducible BdpA expression plasmids were constructed for use in *S. oneidensis*
266 MR-1, *M. atlanticus* CP1, and *E. coli* BL21(DE3) using the pBBR1-mcs2 backbone
267 described previously[60]. The Marionette sensor components (*phlF* promoter, consitutively
268 expressed PhlF repressor, and yellow fluorescence protein (YFP)) cassette from
269 pAJM.452[57] was cloned into the pBBR1-mcs2 backbone, and the YFP cassette was
270 replaced with the gene encoding BdpA by Gibson assembly (primers in Supplemental
271 Table 1). The resulting plasmid was given the name p452-*bdpA*. The Gibson assembly
272 reactions were electroporated into *E. coli* Top10 DH5α cells (Invitrogen), and the
273 sequences were confirmed through Sanger sequencing (Eurofins genomics). Plasmid
274 constructs were chemically transformed into conjugation-competent *E. coli* WM3064 cells

275 for conjugative transfer into the recipient bacterial strains of *S. oneidensis* MR-1 and *M.*
276 *atlanticus* CP1. The same BdpA expression vector was transformed into *E. coli*
277 BL21(DE3) cells (Invitrogen) by chemical transformation.

278 Generation of a scarless *ΔbdpA* knockout mutant of *S. oneidensis* was performed
279 by combining 1 kilobase fragments flanking upstream and downstream from *bdpA* by
280 Gibson assembly into the pSMV3 suicide vector. The resultant plasmid pSMV3_1507KO
281 was transformed into *E. coli* UQ950 cells for propagation. Plasmid sequences were
282 confirmed by Sanger sequencing before chemical transformation into *E. coli* UQ950 for
283 conjugation into *S. oneidensis*. Conjugation of pSMV3_1507KO into *S. oneidensis* MR-
284 1 was performed as described previously[31].

285 **Purification of Outer Membrane Vesicles** *S. oneidensis* MR-1 cells were grown in LB
286 in 1L non-baffled flasks at 30° C at 200 RPM. When an OD_{600} of 3.0 was reached, cells
287 were pelleted by centrifugation at 5000 x g for 20 min at 4°C, resulting supernatant was
288 filtered through a 0.45 µm filter to remove remaining bacterial cells. Vesicles were
289 obtained by centrifugation at 38,400 x g for 1 h at 4°C in an Avanti J-20XP centrifuge
290 (Beckman Coulter, Inc). Pelleted vesicles were resuspended in 20 ml of 50 mM HEPES
291 (pH 6.8) and filtered through 0.22 µm pore size filters. Vesicles were again pelleted as
292 described above and finally resuspended in 50 mM HEPES, pH 6.8, except for vesicle
293 preparations used for electrochemistry which were suspended in 100 mM MES, 100 mM
294 KCl, pH 6.8. Extracellular DNA, flagella, and pili can all be co-purified. Protocol was
295 adapted from[67].

296 **Dynamic Light Scattering** Distribution of vesicle diameters were measured with Wyatt
297 Technology's Möbiuζ dynamic light scattering instrument.

298 **Electrochemistry** CHA Industries Mark 40 e-beam and thermal evaporator was used to
299 deposit a 5 nm Ti adhesion layer and then a 100 nm Au layer onto cleaned glass
300 coverslips (43X50 NO. 1 Thermo Scientific Gold Seal Cover Glass, Portsmouth NH,
301 USA). Self-assembled monolayers were formed by incubated the gold coverslip in a
302 solution of 1mM 6-mercaptohexanoic acid in 200 proof ethanol for at least 2 hours.
303 Electrode was then rinsed several time in ethanol followed by several rinses in milliQ
304 water. The SAMs layer was then activated by incubation in 100 mM N-(3-
305 Dimethylaminopropyl)-N′-ethylcarbodiimide hydrochloride and 25 mM N-
306 hydroxysuccinimide, pH 4, for 30 minutes. A sample of outer membrane vesicles was
307 deposited on the surface of the electrode and incubated at room temperature overnight
308 in a humid environment. Cyclic voltammetry was performed in a 50 mL 3 electrode half-
309 cell completed with a platinum counter electrode, and a 1 M KCl Ag/AgCl reference
310 electrode electrical controlled by a Gamry 600 potentiostat (Gamry, Warminster, PA).
311 The whole experiment was completed in an anaerobic chamber with 95% nitrogen, 5%
312 hydrogen atmosphere.

313 **Proteomics** Vesicle samples were prepared as described above. *S. oneidensis* outer
314 membrane (OM) was purified via the Sarkosyl method described by Brown et al.[68]. A 50
315 mL overnight culture of cells was harvested by centrifugation at 10,000 × g for 10 min.
316 The cell pellet suspended in 20 mL of 20 mM ice-cold sodium phosphate (pH 7.5) and
317 passed four times through a French Press (12000 lb/in^2). The lysate was centrifuged at
318 5,000 × g for 30 min to remove unbroken cells. The remaining supernatant was
319 centrifuged at 45,000 × g for 1 h to pellet membranes. Crude membranes were
320 suspended in 20 mL 0.5% Sarkosyl in 20 mM sodium phosphate and shaken horizontally
321 at 200 rpm for 30 min at room temperature. The crude membrane sample was centrifuged
322 at 45,000 × g for 1 h to pellet the OM. The pellet of OM was washed in ice-cold sodium
323 phosphate and recentrifuged.

324 To prepare for mass spectrometry samples were treated sequentially with urea,
325 TCEP, iodoactinamide, lysl endopeptidase, trypsin, and formic acid. Peptides were then
326 desalted by HPLC with a Microm Bioresources C8 peptide macrotrap (3x8mm). The
327 digested samples were subjected to LC-MS/MS analysis on a nanoflow LC system,
328 EASY-nLC 1200, (Thermo Fisher Scientific) coupled to a QExactive HF Orbitrap mass
329 spectrometer (Thermo Fisher Scientific, Bremen, Germany) equipped with a Nanospray
330 Flex ion source. Samples were directly loaded onto a PicoFrit column (New Objective,
331 Woburn, MA) packed in house with ReproSil-Pur C18AQ 1.9 um resin (120A° pore size,
332 Dr. Maisch, Ammerbuch, Germany). The 20 cm x 50 µm ID column was heated to 60°
333 C. The peptides were separated with a 120 min gradient at a flow rate of 220 nL/min.
334 The gradient was as follows: 2–6% Solvent B (7.5 min), 6-25% B (82.5 min), and 25-40%
335 B (30 min) and to 100% B (9min). Solvent A consisted of 97.8% H2O, 2% ACN, and

336 0.2% formic acid and solvent B consisted of 19.8% H2O, 80% ACN, and 0.2% formic
337 acid. The QExactive HF Orbitrap was operated in data dependent mode with the Tune
338 (version 2.7 SP1build 2659) instrument control software. Spray voltage was set to 2.5
339 kV, S-lens RF level at 50, and heated capillary at 275 °C. Full scan resolution was set to
340 60,000 at m/z 200. Full scan target was 3 × 106 with a maximum injection time of 15 ms.
341 Mass range was set to 300−1650 m/z. For data dependent MS2 scans the loop count
342 was 12, target value was set at 1 × 105, and intensity threshold was kept at 1 × 105.
343 Isolation width was set at 1.2 m/z and a fixed first mass of 100 was used. Normalized
344 collision energy was set at 28. Peptide match was set to off, and isotope exclusion was
345 on. Data acquisition was controlled by Xcalibur (4.0.27.13) and all data was acquired in
346 profile mode.

347 **Bioinformatics** Putative BAR domain SO_1507 (BdpA) was identified in search of
348 annotation terms of *S. oneidensis* MR-1. The conserved domain database (CDD-
349 search)(NCBI) was accessed to identify the position-specific scoring matrix (PSSM) that
350 matched and specific region of SO_1507 that represented the BAR domain. It was
351 confirmed that a region 276-421 matched to BAR superfamily cl12013 and specifically to
352 the family member BAR cd07307. LOGICOIL multi-state coiled-coil oligomeric state
353 prediction was used to determine the presence of coiled-coils within BdpA. SignalP 6.1
354 was used to detect the presence of the signal peptide and cellular localization of BdpA.

355 A PSI-BLAST[69] search against the NCBI nr database was performed using the
356 BdpA BAR sequence as the initial search seed to determine how prevalent the BdpA BAR
357 domain is in related species. Conserved BdpA orthologs were annotated as hypothetical
358 proteins in all of the species identified. In the initial round, 24 proteins were found from

359 other organisms identified as *Shewanella* with a high conservation among the proteins
360 and another 28 proteins were found in more distant bacteria species that had similarity of
361 65% to 44 %. A second iteration identified a few proteins much more distantly related
362 from bacterial species and then proteins from eukaryote phylum *Arthropoda* that were
363 annotated as being centrosomal proteins. All of the found proteins from bacterial species
364 were hypothetical proteins with no known function. Only five of the proteins from the
365 search returned hits to the PSSM of the BAR cd07307. The identity among the proteins
366 was very high and examination of the proteins suggests that a functional form similar to
367 the BAR domain would result for all the found proteins. Overall this places the original
368 protein SO_1507 as a protein that just barely meets criteria via PSSM models to be
369 assigned a matching the BAR domain while the rest of the proteins found have enough
370 differences to fail to match the BAR model while still being very similar to SO_1507. An
371 attempt was made to build up a HMM (Hidden Markov Model) using HMMer to use for
372 searching for other proteins that might match but as with the PSI-BLAST search only the
373 proteins that formed the model returned as good matches. So there appear to be a tight
374 clade of very similar proteins with very little differentiation in the sequence. This indicates
375 that while sequence homology between BdpA and the existing BAR domain consensus
376 sequence predicted the BAR domain region in BdpA using hmmer or NCBI tools, the
377 sequence conservation is at the cusp of a positive hit by the HMM since other closely
378 related (>90% homology) BdpA orthologs were not predicted to contain a BAR domain
379 by this method. The most homologous eukaryotic protein to BdpA (27%) is a putative
380 centrosomal protein in *Vollenhovia emeryi* (accession #: XP_011868153) that is predicted
381 to contain an amino terminal C2 membrane binding domain and a carboxy-terminal SMC

382 domain within a coiled-coil region. Despite CDD search failing to predict the presence of
383 a BAR domain in this protein, it does not preclude the presence of one, pending an
384 updated BAR pfam HMM.

385

386 **Confocal microscopy** For *in vivo* imaging of intrinsic outer membrane extension
387 production, *S. oneidensis* MR-1 strains were grown in LB media overnight, washed twice
388 with SDM, and diluted to an OD_{600} of 0.05 in 1 mL of SDM with appropriate antibiotics.
389 Prior to pipetting, ~1cm of the pipette tip was trimmed to minimize shear forces during
390 transfer. 100 µL of each culture was labeled with 1 µL 1M FM 4-64 to visualize the cell
391 membranes. After staining, 10 µL of the labeled cell suspension was gently pipetted onto
392 22 x 22 mm No.1 cover glass (VWR) and sealed onto glass slides with clear acrylic nail
393 polish (for confocal imaging) or onto chambered cover glass (for widefield fluorescence).
394 On average, intrinsic membrane extension formation could be observed starting after 45
395 minutes sealed onto cover glass. Diluted cells were induced with 12.5 µM DAPG for 1
396 hour at 30˚C with 200 RPM shaking agitation for planktonic OME production. Cells were
397 labeled with FM 4-64 and sealed onto glass slides as before. Induced OMEs were imaged
398 immediately after mounting onto slides.

399 Confocal images were taken by a Zeiss LSM 800 confocal microscope with a Plan-
400 Apochromat 63x/1.4 numerical aperture oil immersion M27 objective. FM 4-64
401 fluorescence was excited at 506 nm: 0.20% laser power. Emission spectra was detected
402 from 592-700 nm using the LSM 800 GaAsP-Pmt2 detector. To capture the dynamics of
403 the OMEs, images were collected over the designated length of time between 0.27 – 0.63
404 seconds per frame. Single frame time series images were collected of either a 50.71 µm

405 by 50.71 μm (2x zoom) or a 20.28 μm by 20.28 μm (5x zoom) field of view. Images were
406 recorded using the Zeiss Zen software (Carl Zeiss Microscopy, LLC, Thornwood, NY,
407 USA).

408 **Perfusion flow microscopy** For OME statistics comparing *S. oneidensis* strains MR-1
409 and Δ*bdpA,* cells were pre-grown aerobically from frozen (-80°C) stock in 10 mL of Luria-
410 Bertani (LB) broth (supplemented with 50 μg/mL Kanamycin for strains with plasmid) in a
411 125-mL flask overnight at 30°C and 225 rpm. The next day, the stationary phase (OD_{600}
412 3.0 – 3.3) preculture was used to inoculate 1:100 into 10 mL of fresh LB medium in a 125-
413 mL flask. After ~6 hours at 30°C and 225 rpm, when the OD_{600} was 2.4 (late log phase),
414 5 mL of cells were collected by centrifugation at 4226 x *g* for 5 min and washed twice in
415 defined medium. The perfusion chamber, microscope, and flow medium described
416 previously[7,29,30] were used for all perfusion flow OME statistics experiments. During each
417 5 hour imaging experiment, the perfusion chamber was first filled with this flow medium,
418 then <1 mL of washed cells were slowly injected for a surface density of ~100-300 cells
419 per 112 x 112 μm field of view on a Nikon Ti-E inverted microscope. Cells were allowed
420 to attach for 5-15 minutes on the coverslip before perfusion flow was resumed at a
421 volumetric flow rate of 6.25 ± 0.1 μL/s. Cells and OMEs were visualized with the red
422 membrane stain FM 4-64FX in the flow medium (0.25 μg/mL of flow medium). A total of
423 1,831 wild type and 2,265 Δ*bdpA* cells were used for extension and vesicle quantification.

424

425 **Cryo transmission electron microscopy**

426 *Shewanella* strains were streaked onto LB plates with or without kanamycin and allowed
427 to incubate 3 days on a benchtop. The night before freezing, individual colonies were

428 inoculated into 3 ml LB +/- kanamycin and incubated at 30 °C overnight with 200 rpm
429 shaking. The following morning optical densities of the cultures were measured at
430 600nm and adjusted to a final OD_{600} of 1. Cells were pelleted at 8,000 rpm for three
431 minutes for buffer exchange/washes. For the Δ*bdpA*_p452-*bdpA* transformed cells, 12.5
432 μM DAPG was added. A freshly glow discharged 200 mesh copper grid with R2/1
433 Quantifoil carbon film was placed into a concavity slide. Approximately 150 μl of a 1:10
434 dilution of the cell suspensions, with or without the inducer, was added to cover the grid.
435 A glass coverslip was then lowered onto the concavity to exclude air bubbles. The
436 edges of the coverslip were then sealed with nail polish to prevent media evaporation.
437 The slide assembly was then incubated in a 30 °C incubator for 1.5 to 3 hours.
438 Immediately prior to plunge freezing, the top coverslip was removed by scoring the nail
439 polish with a razor blade. TEM grids with cells were gently retrieved with forceps and
440 loaded into a Leica grid plunge for automated blotting and plunging into LN_2-cooled
441 liquid ethane. Vitrified grids were transferred to a LN_2 storage dewar. Imaging of frozen
442 samples was performed on either a Titan (ThermoFisher Scientific) microscope
443 equipped with a Gatan Ultrascan camera and operating at 300 kV or a Talos
444 (ThermoFisher Scientific) equipped with a Ceta camera and operating at 200 kV.
445 Images were acquired at 10,000 to 20,000 X magnification and were adjusted by
446 bandpass filtering.

447

448 **Acknowledgements**

449 We thank Dr. Jeffery Gralnick for helpful discussions and advice; Dr. Adam Meyer
450 and Dr. Chris Voigt for the DAPG-inducible Marionette promoter; Dr. Annie Moradian and

Dr. Mike Sweredoski and the California Institute of Technology Proteome Exploration Lab for useful discussions on the preparation and analysis of proteomics data. Some of the cryo-TEM work was done in the Beckman Institute Resource Center for Transmission Electron Microscopy at Caltech. This work was supported by the United States Department of Defense Synthetic Biology for Military Environments (SBME) Applied Research for the Advancement of Science and Technology Priorities (ARAP) program. Work in ME-N's lab was supported by the U.S. Office of Naval Research Multidisciplinary University Research Initiative Grant No. N00014-18-1-2632. LAZ was partially supported by the National Science Foundation grant DEB-1542527. SX was supported by the Division of Chemical Sciences, Geosciences, and Biosciences, Office of Basic Energy Sciences of the U.S. Department of Energy through grant DE-FG02-13ER16415. Work in GJJ's lab was supported by the National Institute of Health (GM122588 to GJJ).

Author Contributions

DP and LZ conceived the study independently then combined projects when complementary data on BdpA was discovered. LZ purified OMVs, prepared samples for LC MS-MS, and performed DLS measurements. LZ and SX made electrochemical measurements and analysis. DP conducted BdpA domain prediction and validation analysis, generated the p452-*bdpA* plasmid, Δ*bdpA* and p452-*bdpA* strains. DP and GC conducted fluorescence and confocal imaging experiments, and DP, LZ, and GC analyzed the data. LB adapted the Marionette sensor (P_{phlF}-YFP) into pBBR1-mcs2. LZ and LAM performed cryo-TEM of OMVs. GC conducted perfusion flow imaging experiments. GC and LZ analyzed perfusion flow system data. CH, DP, and LD performed cryo-TEM experiments of OMEs and image processing / analysis. DP and AM

474 generated phylogenetic data, and DP, AM, and BE analyzed the data. DP, LZ, CM, GC,
475 AM, LAM, BE, GJJ, LD, MEN, and SG provided data interpretation. DP, LZ, MEN, and
476 SG wrote the manuscript, with input from all coauthors.

477

478 ## References

479 1 Carman, P. J. & Dominguez, R. BAR domain proteins-a linkage between cellular membranes,
480 signaling pathways, and the actin cytoskeleton. *Biophys Rev* **10**, 1587-1604, (2018).
481 2 Schoneberg, J. *et al.* Lipid-mediated PX-BAR domain recruitment couples local membrane
482 constriction to endocytic vesicle fission. *Nat Commun* **8**, 15873, (2017).
483 3 van Weering, J. R. & Cullen, P. J. Membrane-associated cargo recycling by tubule-based
484 endosomal sorting. *Semin Cell Dev Biol* **31**, 40-47, (2014).
485 4 Knaevelsrud, H. *et al.* Membrane remodeling by the PX-BAR protein SNX18 promotes
486 autophagosome formation. *J Cell Biol* **202**, 331-349, (2013).
487 5 Mim, C. & Unger, V. M. Membrane curvature and its generation by BAR proteins. *Trends*
488 *Biochem Sci* **37**, 526-533, (2012).
489 6 Rao, Y. & Haucke, V. Membrane shaping by the Bin/amphiphysin/Rvs (BAR) domain protein
490 superfamily. *Cell Mol Life Sci* **68**, 3983-3993, (2011).
491 7 Chong, G. W., Pirbadian, S. & El-Naggar, M. Y. Surface-Induced Formation and Redox-Dependent
492 Staining of Outer Membrane Extensions in Shewanella oneidensis MR-1. *Frontiers in Energy*
493 *Research* **7**, (2019).
494 8 Fischer, T. *et al.* Biopearling of Interconnected Outer Membrane Vesicle Chains by a Marine
495 Flavobacterium. *Appl Environ Microbiol* **85**, (2019).
496 9 Toyofuku, M., Nomura, N. & Eberl, L. Types and origins of bacterial membrane vesicles. *Nature*
497 *Reviews Microbiology*, (2018).
498 10 Hampton, C. M. *et al.* The Opportunistic Pathogen Vibrio vulnificus Produces Outer Membrane
499 Vesicles in a Spatially Distinct Manner Related to Capsular Polysaccharide. *Front Microbiol* **8**,
500 2177, (2017).
501 11 Kim, E. Y., Tyndall, E. R., Huang, K. C., Tian, F. & Ramamurthi, K. S. Dash-and-Recruit Mechanism
502 Drives Membrane Curvature Recognition by the Small Bacterial Protein SpoVM. *Cell Syst* **5**, 518-
503 526 e513, (2017).
504 12 Cornejo, E., Subramanian, P., Li, Z., Jensen, G. J. & Komeili, A. Dynamic Remodeling of the
505 Magnetosome Membrane Is Triggered by the Initiation of Biomineralization. *MBio* **7**, e01898-
506 01815, (2016).
507 13 Bohuszewicz, O., Liu, J. & Low, H. H. Membrane remodelling in bacteria. *J Struct Biol* **196**, 3-14,
508 (2016).
509 14 Remis, J. P. *et al.* Bacterial social networks: structure and composition of Myxococcus xanthus
510 outer membrane vesicle chains. *Environ Microbiol* **16**, 598-610, (2014).
511 15 Wei, X., Vassallo, C. N., Pathak, D. T. & Wall, D. Myxobacteria produce outer membrane-
512 enclosed tubes in unstructured environments. *J Bacteriol* **196**, 1807-1814, (2014).
513 16 Low, H. H., Sachse, C., Amos, L. A. & Lowe, J. Structure of a bacterial dynamin-like protein lipid
514 tube provides a mechanism for assembly and membrane curving. *Cell* **139**, 1342-1352, (2009).
515 17 Peter, B. J. *et al.* BAR domains as sensors of membrane curvature: the amphiphysin BAR
516 structure. *Science* **303**, 495-499, (2004).
517 18 Frost, A., De Camilli, P. & Unger, V. M. F-BAR proteins join the BAR family fold. *Structure* **15**, 751-
518 753, (2007).
519 19 Shimada, A. *et al.* Curved EFC/F-BAR-domain dimers are joined end to end into a filament for
520 membrane invagination in endocytosis. *Cell* **129**, 761-772, (2007).

521 20 Weissenhorn, W. Crystal structure of the endophilin-A1 BAR domain. *J Mol Biol* **351**, 653-661,
522 (2005).
523 21 Drin, G. & Antonny, B. Amphipathic helices and membrane curvature. *FEBS Lett* **584**, 1840-1847,
524 (2010).
525 22 Seet, L. F. & Hong, W. The Phox (PX) domain proteins and membrane traffic. *Biochim Biophys*
526 *Acta* **1761**, 878-896, (2006).
527 23 Itoh, T. & De Camilli, P. BAR, F-BAR (EFC) and ENTH/ANTH domains in the regulation of
528 membrane-cytosol interfaces and membrane curvature. *Biochim Biophys Acta* **1761**, 897-912,
529 (2006).
530 24 Simunovic, M., Voth, G. A., Callan-Jones, A. & Bassereau, P. When Physics Takes Over: BAR
531 Proteins and Membrane Curvature. *Trends Cell Biol* **25**, 780-792, (2015).
532 25 Mim, C. *et al.* Structural basis of membrane bending by the N-BAR protein endophilin. *Cell* **149**,
533 137-145, (2012).
534 26 Habermann, B. The BAR-domain family of proteins: a case of bending and binding? *EMBO*
535 *reports* **5**, 250-255, (2004).
536 27 Miki, H., Yamaguchi, H., Suetsugu, S. & Takenawa, T. IRSp53 is an essential intermediate
537 between Rac and WAVE in the regulation of membrane ruffling. *Nature* **408**, 732-735, (2000).
538 28 Sampath, V., McCaig, W. D. & Thanassi, D. G. Amino acid deprivation and central carbon
539 metabolism regulate the production of outer membrane vesicles and tubes by Francisella. *Mol*
540 *Microbiol* **107**, 523-541, (2018).
541 29 Subramanian, P., Pirbadian, S., El-Naggar, M. Y. & Jensen, G. J. Ultrastructure of Shewanella
542 oneidensis MR-1 nanowires revealed by electron cryotomography. *Proc Natl Acad Sci U S A* **115**,
543 E3246-E3255, (2018).
544 30 Pirbadian, S. *et al.* Shewanella oneidensis MR-1 nanowires are outer membrane and periplasmic
545 extensions of the extracellular electron transport components. *Proc Natl Acad Sci U S A* **111**,
546 12883-12888, (2014).
547 31 Gorby, Y. A. *et al.* Electrically conductive bacterial nanowires produced by Shewanella
548 oneidensis strain MR-1 and other microorganisms. *Proc Natl Acad Sci U S A* **103**, 11358-11363,
549 (2006).
550 32 Bhattacharya, S. *et al.* A Ubiquitous Platform for Bacterial Nanotube Biogenesis. *Cell Rep*, (2019).
551 33 Dubey, G. P. *et al.* Architecture and Characteristics of Bacterial Nanotubes. *Dev Cell* **36**, 453-461,
552 (2016).
553 34 Dubey, G. P. & Ben-Yehuda, S. Intercellular nanotubes mediate bacterial communication. *Cell*
554 **144**, 590-600, (2011).
555 35 Pande, S. *et al.* Metabolic cross-feeding via intercellular nanotubes among bacteria. *Nat*
556 *Commun* **6**, 6238, (2015).
557 36 Tanaka, M., Arakaki, A. & Matsunaga, T. Identification and functional characterization of
558 liposome tubulation protein from magnetotactic bacteria. *Mol Microbiol* **76**, 480-488, (2010).
559 37 Danne, L. *et al.* Membrane Remodeling by a Bacterial Phospholipid-Methylating Enzyme. *MBio*
560 **8**, (2017).
561 38 Danne, L. *et al.* Dissection of membrane-binding and -remodeling regions in two classes of
562 bacterial phospholipid N-methyltransferases. *Biochim Biophys Acta* **1859**, 2279-2288, (2017).
563 39 Danne, L. *et al.* Membrane-binding mechanism of a bacterial phospholipid N-methyltransferase.
564 *Mol Microbiol* **95**, 313-331, (2015).
565 40 Low, H. H. & Lowe, J. A bacterial dynamin-like protein. *Nature* **444**, 766-769, (2006).
566 41 Nealson, K. H. & Scott, J. Ecophysiology of the Genus Shewanella. 1133-1151, (2006).
567 42 Marsili, E. *et al.* Shewanella secretes flavins that mediate extracellular electron transfer.
568 *Proceedings of the National Academy of Sciences* **105**, 3968-3973, (2008).

569 43 Gorby, Y. *et al.* Redox-reactive membrane vesicles produced by Shewanella. *Geobiology* **6**, 232-
570 241, (2008).
571 44 Liu, X. *et al.* Bacterial Vesicles Mediate Extracellular Electron Transfer. *Environmental Science &*
572 *Technology Letters*, (2019).
573 45 Xu, S., Barrozo, A., Tender, L. M., Krylov, A. I. & El-Naggar, M. Y. Multiheme Cytochrome
574 Mediated Redox Conduction through Shewanella oneidensis MR-1 Cells. *J Am Chem Soc* **140**,
575 10085-10089, (2018).
576 46 Okamoto, A., Nakamura, R. & Hashimoto, K. In-vivo identification of direct electron transfer
577 from Shewanella oneidensis MR-1 to electrodes via outer-membrane OmcA–MtrCAB protein
578 complexes. *Electrochimica Acta* **56**, 5526-5531, (2011).
579 47 Cox, J. *et al.* Accurate proteome-wide label-free quantification by delayed normalization and
580 maximal peptide ratio extraction, termed MaxLFQ. *Mol Cell Proteomics* **13**, 2513-2526, (2014).
581 48 Hsu, V. W., Bai, M. & Li, J. Getting active: protein sorting in endocytic recycling. *Nat Rev Mol Cell*
582 *Biol* **13**, 323-328, (2012).
583 49 Vincent, T. L., Green, P. J. & Woolfson, D. N. LOGICOIL--multi-state prediction of coiled-coil
584 oligomeric state. *Bioinformatics* **29**, 69-76, (2013).
585 50 Linkner, J. *et al.* The inverse BAR domain protein IBARa drives membrane remodeling to control
586 osmoregulation, phagocytosis and cytokinesis. *J Cell Sci* **127**, 1279-1292, (2014).
587 51 Cui, H. *et al.* Understanding the role of amphipathic helices in N-BAR domain driven membrane
588 remodeling. *Biophys J* **104**, 404-411, (2013).
589 52 Henne, W. M. *et al.* Structure and analysis of FCHo2 F-BAR domain: a dimerizing and membrane
590 recruitment module that effects membrane curvature. *Structure* **15**, 839-852, (2007).
591 53 Pylypenko, O., Lundmark, R., Rasmuson, E., Carlsson, S. R. & Rak, A. The PX-BAR membrane-
592 remodeling unit of sorting nexin 9. *EMBO J* **26**, 4788-4800, (2007).
593 54 Vinogradov, E., Korenevsky, A. & Beveridge, T. J. The structure of the rough-type
594 lipopolysaccharide from Shewanella oneidensis MR-1, containing 8-amino-8-deoxy-Kdo and an
595 open-chain form of 2-acetamido-2-deoxy-d-galactose. *Carbohydrate Research* **338**, 1991-1997,
596 (2003).
597 55 Toyofuku, M., Tashiro, Y., Hasegawa, Y., Kurosawa, M. & Nomura, N. Bacterial membrane
598 vesicles, an overlooked environmental colloid: Biology, environmental perspectives and
599 applications. *Adv Colloid Interface Sci* **226**, 65-77, (2015).
600 56 Tran, F. & Boedicker, J. Q. Genetic cargo and bacterial species set the rate of vesicle-mediated
601 horizontal gene transfer. *Sci Rep* **7**, 8813, (2017).
602 57 Meyer, A. J., Segall-Shapiro, T. H., Glassey, E., Zhang, J. & Voigt, C. A. Escherichia coli
603 "Marionette" strains with 12 highly optimized small-molecule sensors. *Nat Chem Biol*, (2018).
604 58 Mahmood, M. I., Noguchi, H. & Okazaki, K. I. Curvature induction and sensing of the F-BAR
605 protein Pacsin1 on lipid membranes via molecular dynamics simulations. *Sci Rep* **9**, 14557,
606 (2019).
607 59 Wang, Q. *et al.* Molecular mechanism of membrane constriction and tubulation mediated by the
608 F-BAR protein Pacsin/Syndapin. *Proc Natl Acad Sci U S A* **106**, 12700-12705, (2009).
609 60 Bird, L. J. *et al.* Development of a Genetic System for Marinobacter atlanticus CP1 (sp. nov.), a
610 Wax Ester Producing Strain Isolated From an Autotrophic Biocathode. *Front Microbiol* **9**, 3176,
611 (2018).
612 61 Coursolle, D. & Gralnick, J. A. Modularity of the Mtr respiratory pathway of Shewanella
613 oneidensis strain MR-1. *Mol Microbiol* **77**, 995-1008, (2010).
614 62 Bird, L. J. *et al.* Engineered living conductive biofilms as functional materials. *MRS*
615 *Communications*, 1-13, (2019).

616 63 Ayton, G. S. *et al.* New insights into BAR domain-induced membrane remodeling. *Biophys J* **97**,
617 1616-1625, (2009).
618 64 Simunovic, M. *et al.* Protein-mediated transformation of lipid vesicles into tubular networks.
619 *Biophys J* **105**, 711-719, (2013).
620 65 Noguchi, H. Membrane tubule formation by banana-shaped proteins with or without transient
621 network structure. *Sci Rep* **6**, 20935, (2016).
622 66 Salzer, U., Kostan, J. & Djinovic-Carugo, K. Deciphering the BAR code of membrane modulators.
623 *Cell Mol Life Sci* **74**, 2413-2438, (2017).
624 67 Perez-Cruz, C. *et al.* New type of outer membrane vesicle produced by the Gram-negative
625 bacterium Shewanella vesiculosa M7T: implications for DNA content. *Appl Environ Microbiol* **79**,
626 1874-1881, (2013).
627 68 Brown, R. N., Romine, M. F., Schepmoes, A. A., Smith, R. D. & Lipton, M. S. Mapping the
628 subcellular proteome of Shewanella oneidensis MR-1 using sarkosyl-based fractionation and LC-
629 MS/MS protein identification. *J Proteome Res* **9**, 4454-4463, (2010).
630 69 Altschul, S. F. *et al.* Gapped BLAST and PSI-BLAST: a new generation of protein database search
631 programs. *Nucleic Acids Res* **25**, 3389-3402, (1997).

632

633

634

635

636

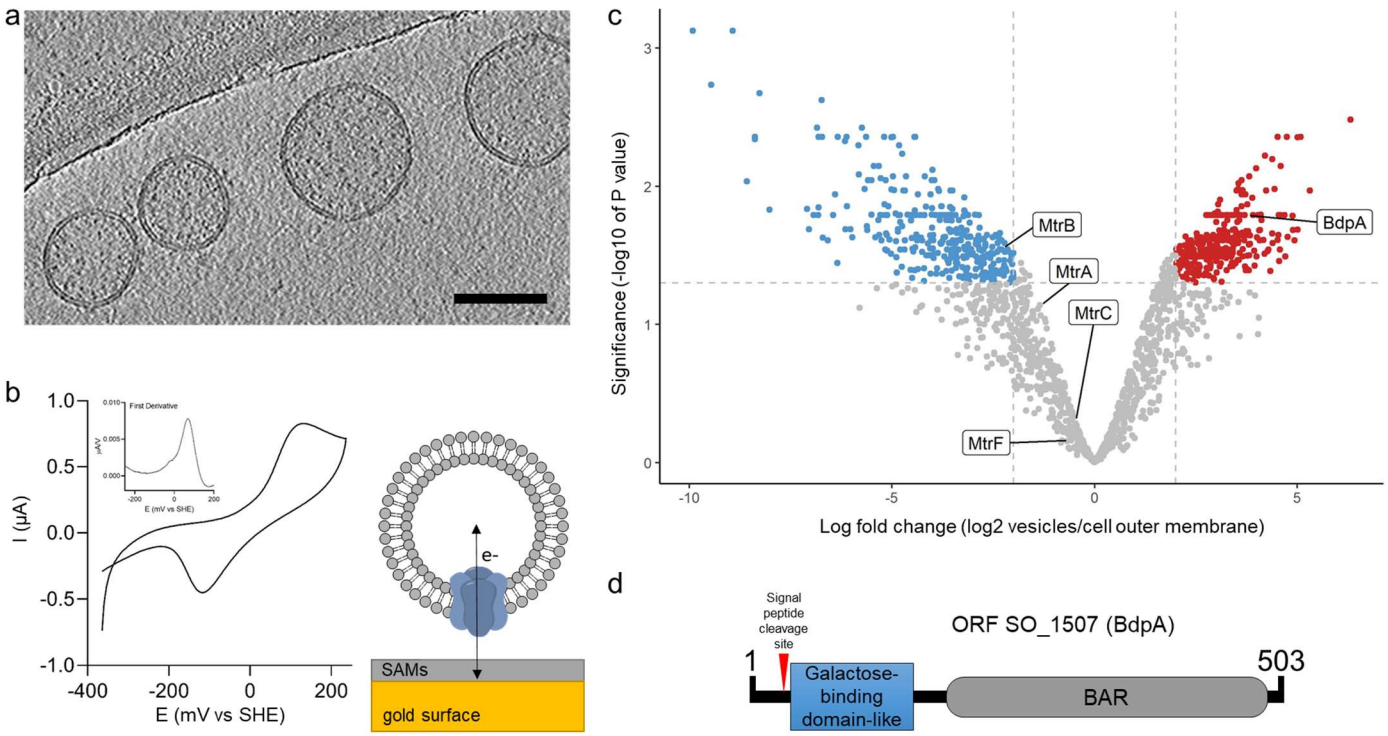

637

638 **Figure 1** Redox active vesicles are enriched with BAR domain protein BdpA. A. Cryo-TEM
639 of *S. oneidensis* MR-1 extra cellular vesicles (scale = 200 nm). B. Cyclic voltammetry of
640 vesicles adhered to gold electrode via small self-assembled monolayers, as diagramed.
641 Inset shows first derivative of anodic scan. C. Volcano plot of vesicle proteome compared
642 to cell-associated outer membrane. D. Schematic of BbdA domains.

643

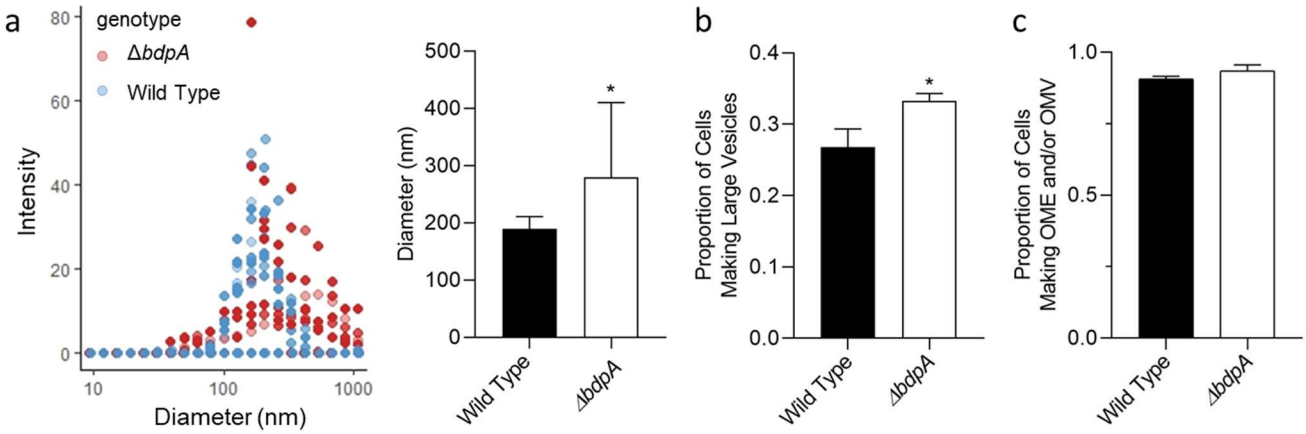

Figure 2 BdpA is responsible for maintaining vesicle morphology but does not alter the frequency of OMV or OME formation. A. Dynamic light scattering of deletion strain compared to wild type, with weighted averages of vesicle size (p = 0.038). B. Quantification of large vesicles being produced by living cells monitored by fluorescence microscopy. C. Quantification of total number of vesicles and extensions being formed by living cells as observed my fluorescence microscopy. Error bars represent standard deviation.

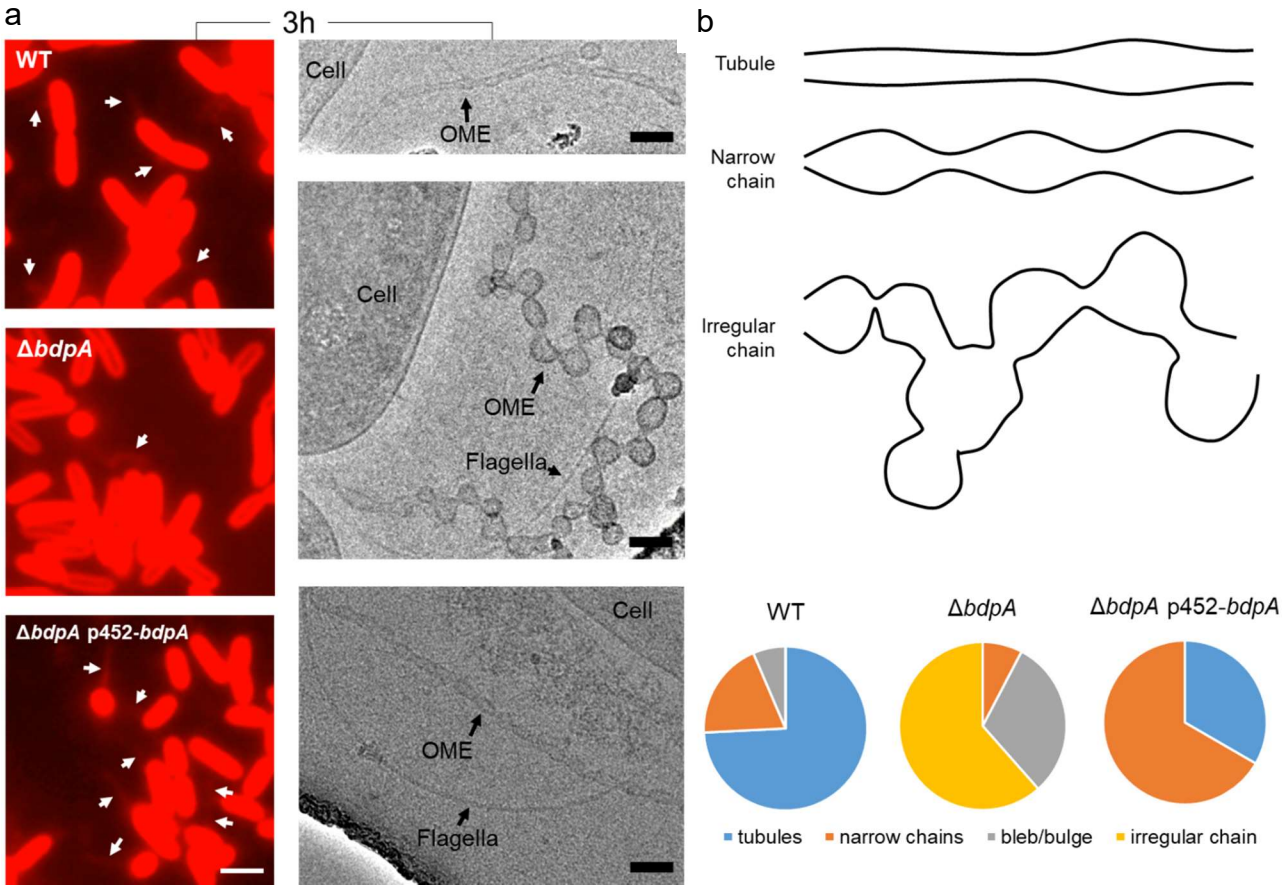

Figure 3 BdpA promotes OME maturation into ordered tubules. A) Fluorescence microscopy (left) and cryo-TEM (right) images of *S. oneidensis* WT (top), Δ*bdpA* (middle), and Δ*bdpA* p452-*bdpA* (bottom) OMEs. Scale = 2 µm (left), 100 nm (right). B) Representative cartoon of OME phenotypes and relative phenotype frequency per outer membrane structure observed from each strain. Membrane blebs/bulges were defined as non-structured membrane protrusions that did not resemble either of the other OME categories.

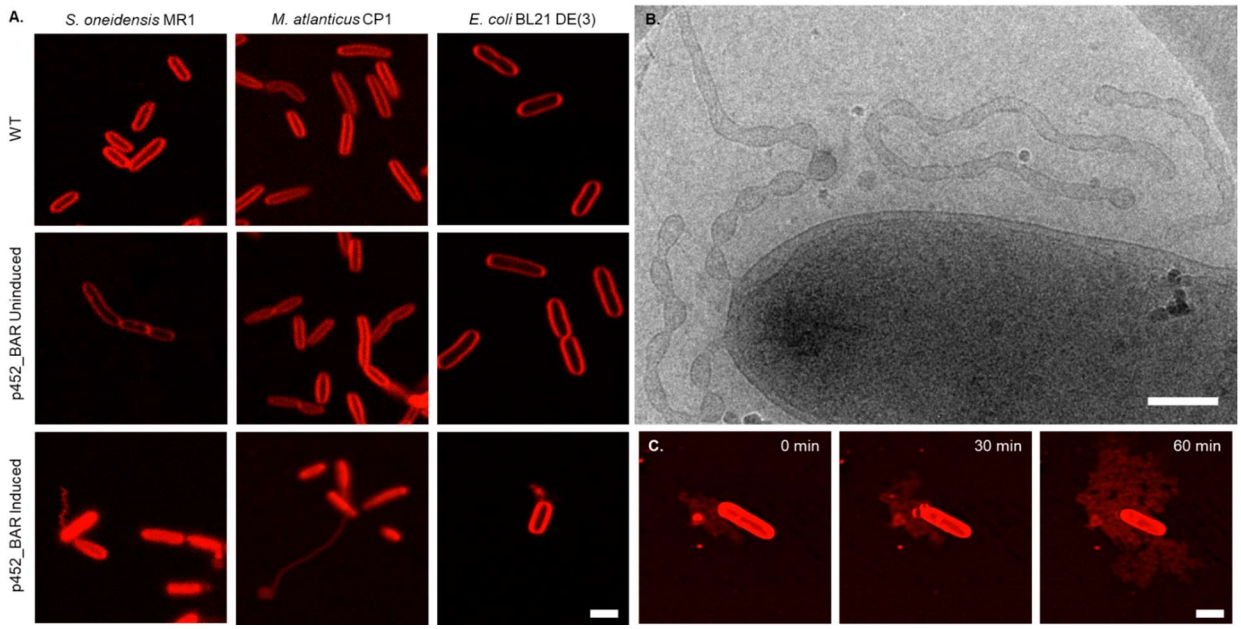

Figure 4 Heterologous expression of BdpA promotes OME formation. A) Induction of BdpA expression during planktonic, non-attached growth results in OME formation in *S. oneidensis* (left), *M. atlanticus* CP1 (middle), and *E. coli* BL21 DE(3) (right). Scale = 2 µm. B) Cryo-TEM image of planktonic *S. oneidensis* OMEs upon induction of BdpA. Scale = 200 nm. C) OME growth over time at 30 minute intervals of *E. coli* BL21 DE(3) expressing BdpA while attached to a glass surface. Scale = 2 µm.

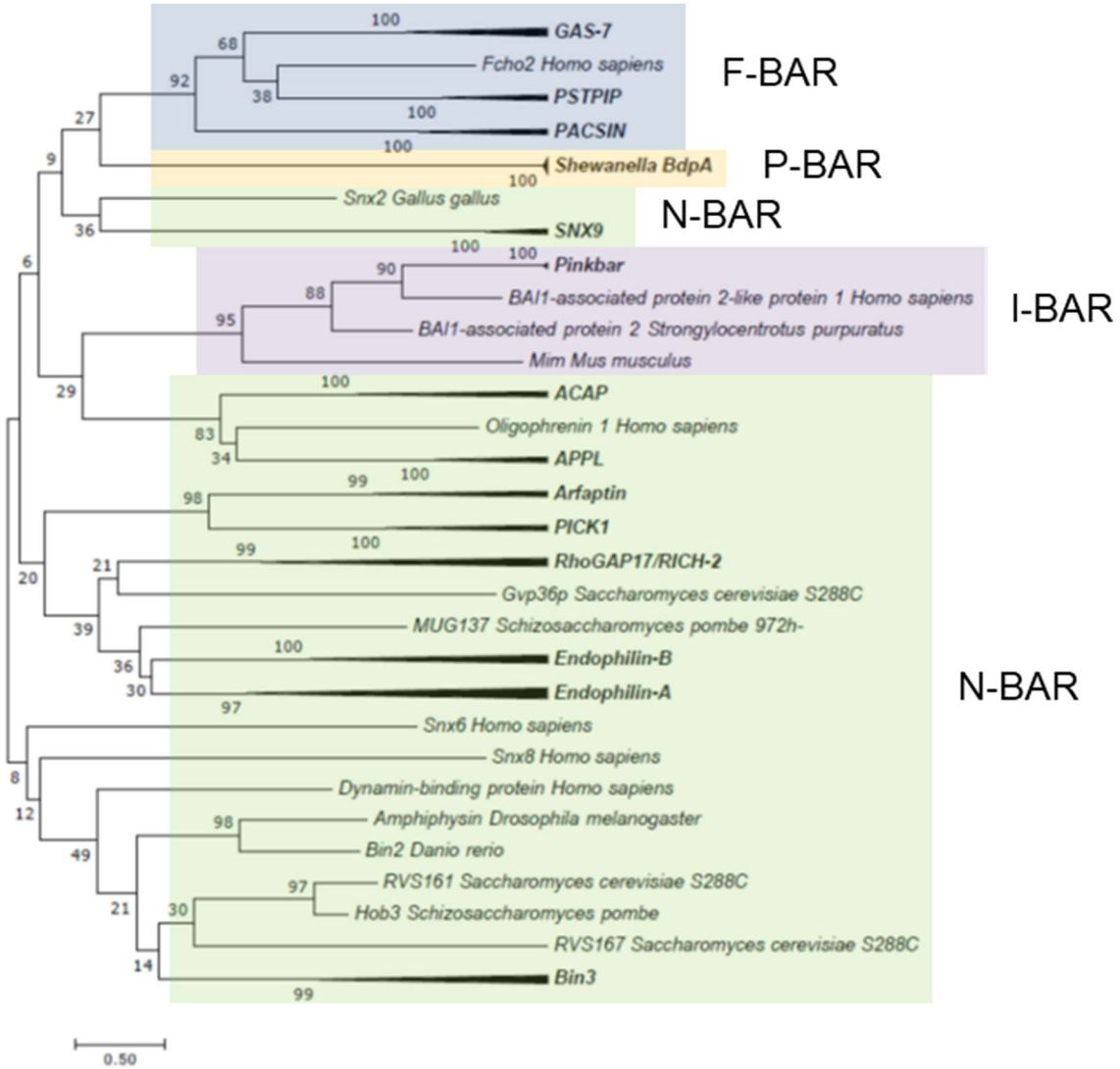

Figure 5 Comparative phylogenetic analysis of BdpA with prokaryotic orthologs and eukaryotic BAR domains. Maximum Likelihood evolutionary histories were inferred from 1000 bootstrap replicates, and the percentage of trees in which the taxa clustered together is shown next to the branches. Arrows indicate multiple branches collapsed to a single node, where arrow height is relative to the number of taxa enclosed within the arrow. *S. oneidensis* BdpA and 5 prokaryotic orthologs (WP_011623497 – unclassified *Shewanella* genus, ESE40074 – *S. decolorationis* S12, WP_039978560 - *S. decolorationis*, KEK29176 – *S. xiamenensis*, and WP_055648003 – *Shewanella sp.* Sh95) predicted by the current BAR domain pfam HMM to contain a BAR domain aligned with representative BAR domains from various BAR domain subtypes (N-BAR, F-BAR, I-BAR).